

HYDROELASTIC RESPONSE OF SUBMERGED FLOATING TUNNEL

A Thesis

by

JIAXING CHEN

Submitted to the Office of Graduate and Professional Studies of
Texas A&M University
in partial fulfillment of the requirements for the degree of

MASTER OF SCIENCE

Chair of Committee,	John Niedzwecki
Committee Members,	Jeffrey Falzarano
	Alan Palazzolo
Head of Department,	Robin Autenrieth

December 2015

Major Subject: Ocean Engineering

Copyright 2015 Jiaxing Chen

ABSTRACT

This research investigation addresses the analysis and numerical simulation of dynamic response of submerged floating tunnels (SFTs) under the influence of surface waves. As an innovative technical solution for waterway crossings, an SFT is usually considered as a slender structure restrained by cable system due to its large aspect ratio, i.e. ratio of length to diameter. Although an SFT is usually placed at a certain depth under the water surface, it is still susceptible to wave field due to its slenderness. In this research study, a three-dimensional finite element solving technique, using both Morison's equation and modal analysis, is formulated to construct a hydroelastic model of an SFT and to determine its deformation considering the fluid-structure interactions. Two preliminary tunnel models for China and Japan, respectively, were studied by implementing the proposed methodology.

In the first case study, a three-dimensional finite element model of the SFT prototype in Qiandao Lake (China) was built in Matlab and subsequently analyzed using mode decomposition to determine its natural frequencies and mode shapes. For each mode shape, Morison's equation was employed to calculate fluid forces at each cross section along the tunnel for given surface wave conditions. Then in the frequency domain, a complex equation of motion was solved iteratively to address the convergence of the stiffness of the cable system. The total dynamic response of SFT was the sum of contributions from each mode component. Results obtained from Matlab were compared with findings from previous publications and numerical simulations in ABAQUS.

Next, a generic pedestrian-aimed SFT proposed for Otaru Crossing in Japan was studied. Parametric studies were performed to evaluate the influence of configuration scheme of cable system and tunnel submerged depth on the dynamic response of SFT. Results show the importance of fundamental structural parameters in the SFT global performance and several key conclusions regarding parameter selections were drawn for engineering practices in design phase.

DEDICATION

To my parents and my wife
For their endless love, support and trust

ACKNOWLEDGEMENTS

It has been a wonderful journey for me to study and pursue my Master's degree in ocean engineering at Texas A&M University. I would like to express my sincere gratitude to Prof. John Niedzwecki for his continuous support of my research study and thesis writing. His patience, motivation, and insightful knowledge has fueled me all the way to the point where I am today. I would also like to thank Prof. Jeffrey Falzarano for his suggestions and comments on my research and Prof. Alan Palazzolo for his efforts of equipping me with solid foundation in finite element analysis.

Besides the aforementioned committee members, I am grateful to Prof. Jun Zhang and Prof. Moo-Hyun Kim for their dedicated work in teaching wave mechanics and non-linear hydrodynamics from which I have learnt a lot. Gratitude also goes to other department faculty and staff for making my time in Aggieland a joyful and memorable experience. I would also like to thank the Ocean Engineering Program at Texas A&M University for offering me financial support over the last two years including British Petroleum Corporation Fellowship and American Bureau of Shipping Scholarship.

In particular, I would like to express my special thanks to Mr. and Mrs. Thompson (former aggies) for helping me get involved in American culture. I am also grateful to my wife, Mrs. Bingjie Chen, and all other family members for their selfless love, trust, patience and support.

NOMENCLATURE

SFT	Submerged Floating Tunnel
BEM	Boundary Element Method
FEM	Finite Element Method
BWR	Buoyancy Weight Ratio
K.C.	Kuelegan-Carpenter
SIJLAB	Sino-Italian Joint Laboratory of Archimedes Bridge
F	Hydrodynamic Force
ρ	Fluid Density
u	Flow Velocity
v	Body Velocity
C_M	Inertia Coefficient
C_D	Drag Coefficient
V	Volume of the Body
A	Cross-section Area
u_{\max}	Amplitude of the Flow Velocity Oscillation
T	Wave Period
L	Characteristic Scale of the Object
$y(x,t)$	Structural Response
x	Position Variable

t	Time Variable
ϕ_i	i th Modal Component
a_i	Principle Modal Coordinate
U	Total Response of SFT
U_s	Static Response
U_D	Dynamic Response
M	Mass Matrix of the Tunnel
K	Stiffness Matrix of the Tunnel
F_D	Hydrodynamic Force Vector
\ddot{U}	Second Derivative of Dynamic Response w.r.t Time
ω	Natural Frequency
d	Mode Shape
D	Modal Matrix
$p(t)$	Time Dependent Principle Coordinate Vector
d_T	Tunnel Diameter
l	Length of Each Segment
Tc	Cable Axial Force
θ	Inclined Angle
E	Young's Modulus
K_h	Equivalent Cable Horizontal Stiffness
K_v	Equivalent Cable Vertical Stiffness

TABLE OF CONTENTS

	Page
ABSTRACT	ii
DEDICATION	iv
ACKNOWLEDGEMENTS	v
NOMENCLATURE	vi
TABLE OF CONTENTS	viii
LIST OF FIGURES	x
LIST OF TABLES	xii
1. INTRODUCTION.....	1
1.1 Overview	1
1.2 Literature Review	4
1.3 Research Objectives	8
2. METHODOLOGY FORMULATION.....	9
2.1 General Morison's Equation	9
2.2 Mode Decomposition	11
2.3 Hydroelastic Model	13
3. IMPLEMENTATION AND VALIDATION.....	17
3.1 SFT Prototype in Qiandao Lake (PR of China)	17
3.1.1 Structural parameters.....	18
3.1.2 Fluid properties.....	20
3.2 Sensitivity Study of Cable Stiffness.....	21
3.3 Numerical Implementation.....	24
3.4 Program Validation	28
3.4.1 Static calculation	28
3.4.2 Dynamic calculation.....	32

	Page
4. APPLICATION.....	37
4.1 Project Description.....	37
4.2 Wave Conditions.....	38
4.3 Structural Model.....	39
4.4 Dynamic Response under Monochromatic Waves	40
4.5 Parametric Study	44
5. SUMMARY	48
REFERENCES.....	50

LIST OF FIGURES

	Page
Figure 1.1 Supporting system of SFT (a) pontoons (b) cables.....	2
Figure 1.2 Illustrations of SFT for (a) transportation (b) recreation	3
Figure 2.1 Flow past a moving cylinder.....	9
Figure 2.2 Illustration of mode decomposition	12
Figure 2.3 Sketch of SFT prototype (Qiandao Lake) in ABAQUS	14
Figure 3.1 (a) A view of Qiandao Lake (b) Location of the SFT prototype	17
Figure 3.2 Schematic sketch of the SFT prototype	18
Figure 3.3 The cross section of the SFT prototype	19
Figure 3.4 Cable configurations for the SFT prototype	19
Figure 3.5 Single-cable system for sensitivity study.....	21
Figure 3.6 Change of horizontal and vertical stiffness due to tunnel's movement	23
Figure 3.7 Sketch of SFT (Config. 3) in ABAQUS	25
Figure 3.8 Sketch of SFT model in Matlab	26
Figure 3.9 Flow chart of stiffness convergence with bisection method.....	26
Figure 3.10 Flow chart of numerical analysis in Matlab.....	27
Figure 3.11 Illustration of static force on SFT	29
Figure 3.12 Static results of configuration 1	29
Figure 3.13 Static results of configuration 2	30
Figure 3.14 Static results of configuration 3	31
Figure 3.15 Dynamic results of configuration 1	33

	Page
Figure 3.16 Dynamic results of configuration 2	33
Figure 3.17 Dynamic results of configuration 3	34
Figure 4.1 Location of Otaru In-port Crossing SFT.....	38
Figure 4.2 Structural parameters of SFT in Otaru.....	39
Figure 4.3 Dynamic results of proposed SFT in Otaru	40
Figure 4.4 Mode percentage in horizontal response	42
Figure 4.5 Cable group and cable number assignments.....	43
Figure 4.6 Variation of cable tension	43
Figure 4.7 Comparison of horizontal response	45
Figure 4.8 Comparison of cable tension variations.....	46

LIST OF TABLES

	Page
Table 1.1 Methodologies Comparison on selected papers	7
Table 3.1 Equivalent structural parameters of tunnel.....	18
Table 3.2 Structural parameters of cable.....	20
Table 3.3 Data of fluid environment	21
Table 3.4 Cable Properties	22
Table 3.5 Cases for Sensitivity Study	23
Table 3.6 Summary of maximum displacement (m) comparison	32
Table 3.7 Summary of response magnitude comparison	35
Table 4.1 Major feasibility studies done by the society of SFT research in Hokkaido...	37
Table 4.2 Equivalent structural parameters of SFT in Otaru	40
Table 4.3 Cases for parametric study	44

1. INTRODUCTION

1.1 Overview

The crossing of waterways has been one of the most complex and challenging issues in civil engineering. Although hundreds of thousands of conventional structures, such as suspension bridges and subsea tunnels, have been built successfully around the world for decades, they have probably reached their maximum level of development and applications. In addition, many problems and disadvantages have arisen for conventional solutions when it comes to long crossing distances, deep water areas, complex seabed morphologies, and severe sea surface conditions. Therefore, a revolutionary solution needs to be conceived and is required to fulfill the needs of increasingly demanding crossing conditions.

Submerged floating tunnels (SFTs), an innovative concept emerging in recent decade, offer the possibility of opening a new chapter of waterway crossings. Unlike subsea tunnels buried under the seabed, SFTs are usually conceived as tubular floating structures to be placed at a pre-fixed depth in the water (See Figure 1.1). According to Archimedes' principle, the force differential between the total buoyancy and the gravitational loads results in the net buoyancy that must be counterbalanced by supporting system distributed along the tunnel. Supporting system can either be pontoons on the surface or cables anchored to the seabed. With proper design configuration, the tension of supporting system provides adequate horizontal and vertical stiffness to stabilize the motions of SFT.

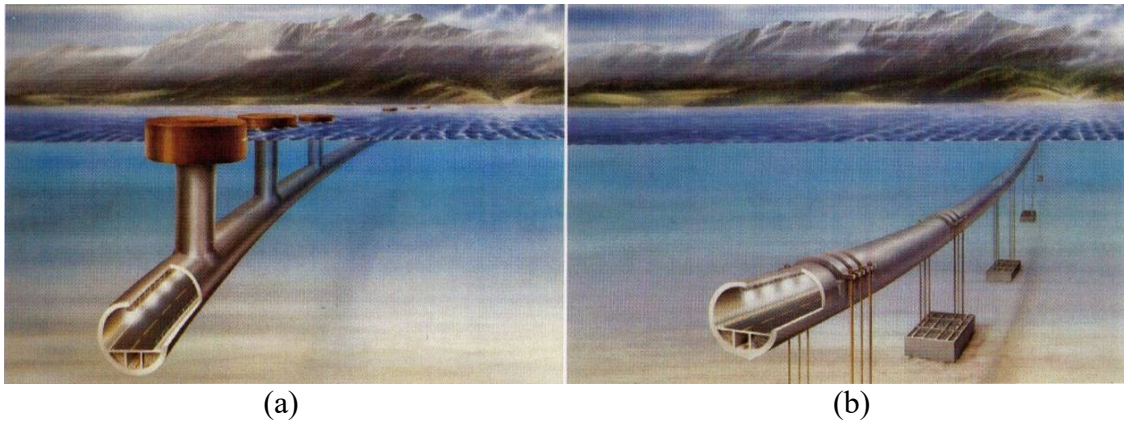


Figure 1.1 Supporting system of SFT (a) pontoons (b) cables ^[1]

Compared with conventional waterway crossing solutions, SFTs feature the following four major advantages. First of all, SFTs are designed as modular structures which makes it stable in every phase of construction and its total cost is approximately proportional to the whole crossing length.^[2] In addition, SFTs with cable anchoring system have little interference with water surface transportation since the tunnels can be submerged to create enough clearance depth. Moreover, SFTs can be flexibly applied to areas with significant changes of seabed slope where subsea tunnel might have difficulty to be constructed. Finally, as a state-of-the-art design concept, SFTs have less negative impact on the beauty of the surrounding environment.

Over the last few decades, SFTs have been envisioned for applications such as vehicle transportation and recreational activities (See Figure 1.2). For SFTs with circular cross section, diameters can range from 3m to 30m, which is influenced by its design purposes and the corresponding design loads. As a consequence of the aforementioned advantages, the length of SFTs can cover a wider range compared with traditional

structures. For example, the design length of Daikokujima Crossing SFT (for pedestrian) is 120m while that of Soya Strait Crossing SFT (for vehicle & railroad) goes up to 43,000m.^[3]



Figure 1.2 Illustrations of SFT for (a) transportation (b) recreation ^[3]

The aspect ratio of an SFT is defined as the ratio of the tunnel length to its characteristic cross-section dimension. This ratio can be as large as 10^2 to 10^3 , which means an SFT can be treated as a slender beam restrained by cable system that responds to environmental loadings. Although an SFT is usually submerged at a certain depth in the water, studies show surface waves still have important influence on its dynamic response due to its slenderness. Moreover, without the assumption of rigid body behavior, the interaction between body deformation and surrounding fluid should be taken into consideration during dynamic analysis.

1.2 Literature Review

Since 1980s, there have been comprehensive studies on conceptual design and dynamic response analysis of SFTs by researchers from Norway, Italy, China, Japan and Korea. However, no SFT has been constructed at this point. The main reason can be identified as the consideration of potential uncertainties yet to be discovered and solved. More and more theoretical and numerical studies, and experimental data are still needed before the realization of the first SFT construction. In the past decades, the evaluations of dynamic behavior of SFTs under various environmental conditions, such as waves, currents, earthquakes, tsunami or accidental loads, have been studied by using theories and methodologies previously applied to classic floating structures.

Wu (1984)^[4], Price et al. (1985)^[5], Bishop et al. (1986)^[6], and Newman (1994)^[7] presented a generalized three-dimensional hydroelasticity theory to study the fluid-structure interaction of arbitrary shape objects in wave fields. Their study adopted a frequency-domain approach, solving for the fluid velocity potential for each mode shape. This methodology was later employed by Ge et al. (2010)^[8] to study the dynamic response of the SFT prototype in Qiandao Lake (PR of China) under wave effects. Dry mode components of SFT were calculated using a three-dimensional finite element method. A boundary element method (BEM) was used to solve for diffraction and radiation potentials. In order to reduce the computational problems associated with the use of a three-dimensional BEM, Paik et al. (2004)^[9] developed a time-domain dynamic analysis program for SFTs under wave field. They simplified the problem by pre-calculating added

mass and radiation damping coefficients using two-dimensional radiation/diffraction theory with BEM approach.

Other researchers utilized Morison's equation for the evaluation of hydrodynamic forces. Brancaloni and Castellanit (1989)^[10] pursued a coupled fluid-structure interaction approach incorporating the general Morison's equation. Lagrangian approach was used to deal with non-linearity of drag force and the solution was solved via direct time integration. Using the same methodology, Long et al. (2009)^[11] found buoyancy weight ratio (BWR) and structural damping are two key factors in terms of SFT dynamic response. With the help of commercial software, Mazzolani et al. (2010)^[12] conducted dynamic analysis via Morison's equation and they found configurations of cable system have significant influence on the maximum response amplitude of SFT.

Based upon the aforementioned studies, it can be concluded that there are mainly two methods for conducting the hydrodynamic analysis of SFTs. One involves using potential radiation/diffraction theory, and the other is Morison's equation (See Table 1.1). According to Kunisu (2010)^[13], both methods show pretty good agreement on calculated wave forces for large K.C. number, in which case it is also recognized that both drag force and inertia force simultaneously work on SFT.

One advantage of potential theory is that it can be applied within the whole range of wave frequencies in a sea state. Pressure distribution over SFT surface can be obtained using Bernoulli's equation and accurate results can be achieved from discretization using sufficient boundary elements. However, it's sometimes very difficult and time consuming to determine velocity potentials for each mode component and more computational power

is needed for large SFTs with long-crossing distances that can be thousands of meters. Morison's equation, therefore, can be used under appropriate condition to simplify the problem. Due to the slenderness of the tunnel, researchers discretize the structure using finite elements and then calculate the drag and inertia force for each section according to fluid-structure relative velocity and acceleration at each time step. However, even utilizing existing commercial software, e.g. ABAQUS^[14] or ANSYS, to conduct time-domain analysis, the computational time grows exponentially as the number of elements increases.

To address these issues, in this research study a different approach combining Morison's equation and mode decomposition is pursued. Mode decomposition is used to identify the dominant modal components for the slender beam. Cable system is modeled as springs attached to corresponding sections along the beam. Once the mode shapes are known, Morison's equation can be applied to calculate fluid forces for each cross section and then the equation of motion is solved in frequency domain to determine the total dynamic response of SFT under wave fields.

Table 1.1 Methodologies Comparison on selected papers

Author(s)	Methodology	SFT Dimensions	Environmental Conditions	Key Conclusions
Brancaleoni and Castellani (1989)	Morison's equation & direct time integration & Lagrangian approach	Elliptic (20x40m) Length (3000m)	Wave height 6.6m Wave period 11.2s Water depth 150m	Spans must be short for severe environments; Inertia & drag terms significant to response
Long et al. (2009)	Morison's equation & frequency-dependent damping coefficients	SFT in Qiandao Lake Circular (D = 4.39m) Length (100m)	Wave height 1.0m Wave period 1.8s Water depth 30m Surface current 1.0m/s	Buoyancy weight ratio & structural damping are key factors in design
Mazzolani, Faggiano, and Martire (2010)	Morison's equation & ABAQUS/Aqua package		Without current effect	Three cable system configurations are compared in terms of displacement, bending moment and axial force
Ge et al. (2010)	Potential theory with BEM & mode decomposition		Axial relaxation device could minimize maximum dynamic response	
Paik et al. (2004)	2-D diffraction theory and BEM are employed to calculate frequency-dependent parameters. Impulse response function is introduced to solve motion equation.	Circular (D = 11.4m) Length (855m)	Wave period varies from 2.25s to 26.46s Maximum wave height 4.08m Water depth 100m	SFT submerged depth affects the dynamic response considerably; The effect of depth on radiation damping is more significant than that on added-mass and the maximum wave force decreases rapidly as SFT depth increases
Kunisu (2010)	Assume 2-D fixed structure. Boundary element method for diffraction theory based on the velocity potential; Morison's equation	Circular (D ranges from 4 to 23m) Elliptic (23x35m)	Wave number varies from 0.01 to 0.16 Water depth 100m	Wave force acting on submerged floating tunnel can be calculated accurately by applying both Morison's equation and Boundary Element Method; Drag force and inertia force simultaneously work on the SFT; Inertia force becomes dominant when K.C. is less than 15 in the case of SFT with larger diameter

1.3 Research Objectives

The objective of this research study was to formulate a procedure for constructing a hydroelastic model of a submerged floating tunnel, designed using a three-dimensional finite element method, and to solve for its dynamic response using a combination of modal analysis and Morison's equation in frequency domain. The site specific wave conditions were modeled as regular waves travelling perpendicular to the longitudinal direction of the tunnel. The large Kuelegan-Carpenter (K.C.) number for the SFT design allowed the application of Morison's equation. Two case studies were conducted as applications of the proposed methodology. The first case study is based on research data of the SFT prototype in Qiandao Lake extracted from publications of Sino-Italian Joint Laboratory of Archimedes Bridge (SIJLAB). The predictions from the new model were compared with previous findings in terms of maximum static and dynamic response for three different anchoring system configurations. The second case study deals with a proposed pedestrian-aimed SFT for the Otaru Crossing project in Japan. Since this proposed SFT has a smaller diameter compared to transportation applications and is located underwater with considerable clearance depth, the radiation damping effect can be neglected. In addition, some parametric studies are conducted to highlight several key structural parameters for SFT preliminary design.

2. METHODOLOGY FORMULATION

2.1 General Morison's Equation

Flow past a circular cylinder, as shown in Figure 2.1, is a classic problem in ocean engineering. For incompressible and inviscid potential flow, the total force acting on a moving body with constant velocity relative to the fluid is zero according to D'Alembert's paradox. For inviscid unsteady flow, the hydrodynamic added mass effect is observed as the surrounding fluid is deflected by the accelerating or decelerating body motion. In addition to added-mass, drag forces resulting from flow separation and boundary layer friction should also be taken into consideration in certain cases.

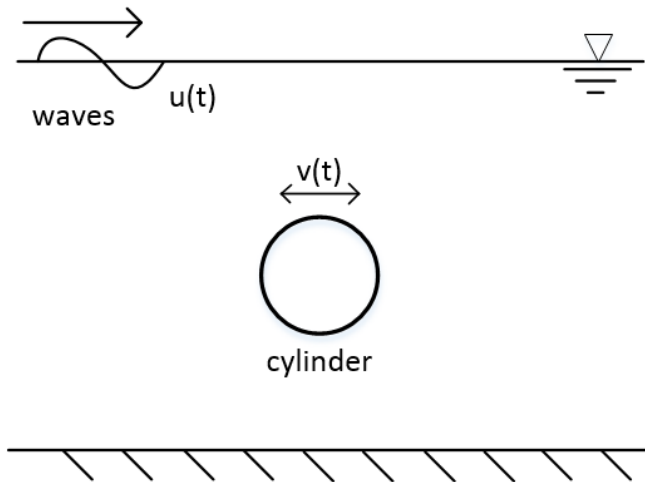


Figure 2.1 Flow past a moving cylinder

Morison's equation was first proposed by Morison, Johnson, and Schaaf (1950)^[15] to describe the hydrodynamic forces on a cylindrical object in an oscillatory flow. For cases when both the body and fluid are moving, a general Morison's equation for a body with unit length is utilized to account for the relative velocity and acceleration.

$$F = \rho V \ddot{v} + \frac{1}{2} \rho C_M A \dot{u} \dot{v} + \frac{1}{2} \rho C_D A |u - v| (u - v) \quad (2.1)$$

where ρ is fluid density, u is the flow velocity, v is the body velocity, C_M is the inertia coefficient, C_D is the drag coefficient, V is the submerged volume of the body, A is the cross-sectional area of the body perpendicular to the flow direction.

Later, Keulegan and Carpenter (1956) defined a dimensionless quantity Kc , Keulegan-Carpenter number, to describe the relative importance of drag forces over inertia forces for bluff objects. As a general rule, the inertia component is dominant for $Kc < 5$ while the drag force becomes more important for $Kc > 15$. Kc is written as:

$$Kc = \frac{u_{\max} T}{L} \quad (2.2)$$

where u_{\max} is the amplitude of the flow velocity oscillation, T is the wave period, L is the characteristic scale of the object in the direction of fluid flow (e.g. the diameter for cylinder).

One assumption of Morison's equation for a cylinder in travelling waves is the diameter of the cylinder is much smaller than the wavelength. This condition limits the range of wave frequencies that allows the use of Morison's equation to evaluate wave forces on the cylinder. According to Vongvisessomjai and Silvester (1976), $Kc > 5$

should be satisfied for good estimates by Morison's equation. For those cases with $Kc < 5$, the potential radiation/diffraction theory should be pursued instead.

2.2 Mode Decomposition

In structural analysis, mode decomposition is often used for dynamic analysis of large structural systems. The main idea is the structural motion can be represented by the sum of a number of mode shapes. In this way, a system with n degrees of freedom (dof) can be reduced to a simplified model with selected number of dof. This reduction in dimensionality is extremely important as it simplifies the problem without loss of significant accuracy and the solving process can be accelerated as it requires less computational power.

If $y(x,t)$ is used to represent the exact solution of structural response, x is the position variable, t is the time variable, ϕ_i ($i = 1, 2, 3, \dots$) is the i th modal component, then $y(x,t)$ can be approximated as:

$$y(x,t) \cong a_1\phi_1 + a_2\phi_2 + a_3\phi_3 + \dots \quad (2.3)$$

where a_1, a_2, a_3, \dots are called principle (modal) coordinates. They are determined by solving uncoupled equations in terms of selected mode shapes. Theoretically speaking, the more number of mode shapes selected, the more accurate the result can be. The visual representation of mode decomposition is shown in Figure 2.2.

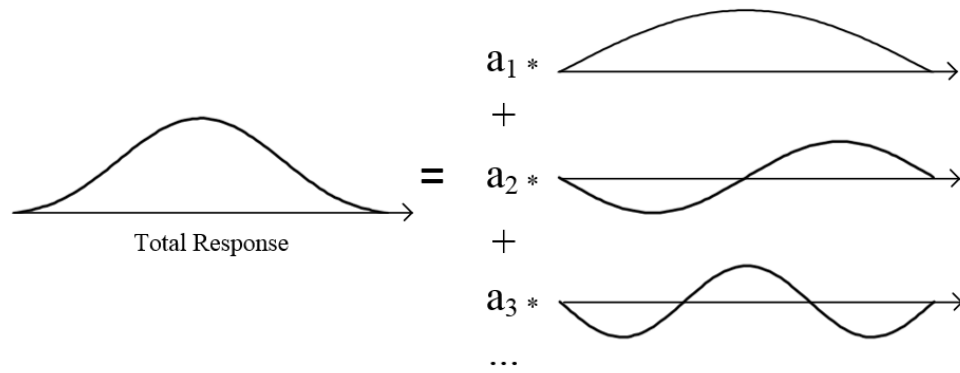


Figure 2.2 Illustration of mode decomposition

This approach is also useful for hydrodynamic study of large slender floating structures such as submerged floating tunnels. For SFTs, usually only the first few modal components corresponding to the lower natural frequencies need to be considered because the wave energy is primarily concentrated at lower frequency range compared with the structural natural frequencies.

As a common practice in hydroelasticity analysis, the dry undamped natural modes are used instead of the wet natural modes. The dry modes correspond to modal components as if the structure were put in air. This method neglects the effects of fluid on structural mode shapes. On the other hand, the wet modes consider not only the mechanical properties of the structure but also the actions of the surrounding fluid. According to Bishop and Price (1976), both of these strategies have some advantages and disadvantages. The dry-mode approach is more preferable because of its simplicity and adaptability for applications of large floating structures. Therefore, in this research paper, the dry-mode approach is utilized to determine the modal components of SFTs.

2.3 Hydroelastic Model

In this section, the procedure for constructing a hydroelastic model of SFT is presented based on three-dimensional finite element method (FEM). For environmental condition, a series of monochromatic waves is travelling perpendicular to the axial direction of the horizontal SFT. General Morison's equation is used to calculate wave forces on slender moving tunnel. The dynamic equation of SFT is decomposed into uncoupled equations using mode decomposition. The principle modal coordinates are solved in frequency domain.

The total response U of an SFT is defined as the transverse displacements in vector form. These displacements are referenced to the straight line connecting the two ends of the tunnel. U can be estimated as the sum of static response U_S and dynamic response U_D .

$$U = U_S + U_D \quad (2.4)$$

The static response U_S is the result of the buoyancy, gravitational loads, and cable axial loads in still water, which can be easily calculated by Matlab (or ABAQUS) using fundamental three-dimensional finite element method. The dynamic structural response U_D is a consequence of the hydrodynamic forces induced by the wave field.

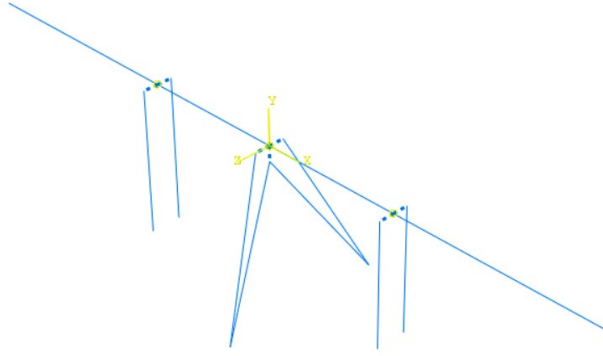


Figure 2.3 Sketch of SFT prototype (Qiandao Lake) in ABAQUS

Assuming that the submerged tunnel (See Figure 2.3) can be modeled using three-dimensional beam elements and the cable system represented as equivalent springs, the undamped dynamic equation of motion of SFT can be written as:

$$M\ddot{U}_D + K U_D = F_D \quad (2.5)$$

where M is the mass matrix of the tunnel, K is the stiffness matrix of the tunnel (including the effect of cable system), F_D is the hydrodynamic force vector. \ddot{U}_D denotes the second derivative of the dynamic response U_D with respect to time.

The dry natural modes of SFT vibration are obtained by solving the homogeneous form of the equation of motion:

$$(-\omega^2 M + K)d = 0 \quad (2.6)$$

where ω is the natural frequency and d is the corresponding mode shape.

Assuming that the first N modes are sufficient to represent the structural response, then

$$\begin{aligned}
U_D &= D \cdot p(t) \\
D &= [d_1 \quad d_2 \quad \dots \quad d_N]
\end{aligned}
\tag{2.7}$$

where D is the modal matrix containing the first N components, and $p(t)$ is the time dependent principle coordinate vector which reflects the magnitude for each natural mode.

When both the tunnel and fluid are moving, the general Morison's equation is written as:

$$F_D(t) = \rho C_M \frac{\pi}{4} d_T^2 l \dot{u}(t) + \rho C_D \frac{\pi}{4} d_T^2 l u(t) |u(t)|
\tag{2.8}$$

where C_M is the inertia coefficient and C_D is the drag coefficient, ρ is the fluid density and $u(t)$ is the fluid velocity, d_T is the tunnel diameter and l is the length of each segment.

Once the SFT is discretized into segments, then for each segment, the general Morison's equation is applied. The calculated hydrodynamic force consists of three components.

$$F_D^e = F_{inertia}^e + F_{added}^e + F_{drag}^e
\tag{2.9}$$

The superscript of e denotes element-wise variant.

It follows then that

$$\begin{aligned}
F_{drag}^e &= C_D \frac{1}{2} \rho d_T l^e (u^e(t) - U) |u^e(t) - U| \\
u^e(t) &= \begin{bmatrix} u_1^e \\ u_2^e \end{bmatrix} = \bar{u}^e \begin{bmatrix} e^{i\frac{\pi}{2}} \\ 1 \end{bmatrix} e^{-i\omega t} \\
U_D^e(t) &= D^e \bar{p}^e e^{-i\omega t}
\end{aligned}
\tag{2.10}$$

where \bar{p}^e is a time-independent element-wise principle coordinate vector whose entries are usually complex values.

Assuming that $|u(t)| \gg \dots$, which is generally true according to several research findings, this simplifies the quadratic velocity term in F_{drag}^e as follows:

$$\begin{aligned}
 & (u^e(t) - \dot{U})^2 \\
 &= u^e(t) |u^e(t) - \dot{U}| \\
 &\cong u^e(t) |u^e(t) - \dot{U}|
 \end{aligned} \tag{2.11}$$

Collecting all the terms and substituting them into the dynamic equation of motion, the principle coordinate vector \bar{p} can be determined, and the structural dynamic response can be evaluated as:

$$U_D(t) = D\bar{p}e^{-i\omega t} \tag{2.12}$$

The total response can then be obtained by adding static response as:

$$U(t) = U_S + U_D(t) \tag{2.13}$$

3. IMPLEMENTATION AND VALIDATION

3.1 SFT Prototype in Qiandao Lake (PR of China)

As a case study, the SFT prototype in Qiandao Lake is selected to implement and validate the proposed methodology (See Figure 3.1). The SFT prototype is an ongoing project investigated by researchers from the Sino-Italian Joint Laboratory for Archimedes Bridge (SIJLAB). Since 2004, they have been using both pure Morison's equation and potential theory with BEM to determine structural response in the presence of environmental loadings. Structural dimensions and numerical results are available from recent publications, which will be discussed in detail in the following sections.



Figure 3.1 (a) A view of Qiandao Lake (b) Location of the SFT prototype ^[12]

3.1.1 Structural parameters

The total length of the SFT prototype is 100m. It consists of five segments that is 20m long each. Three cable groups are deployed at the mid-span of the middle three segments. A schematic sketch of the SFT is shown in Figure 3.2.

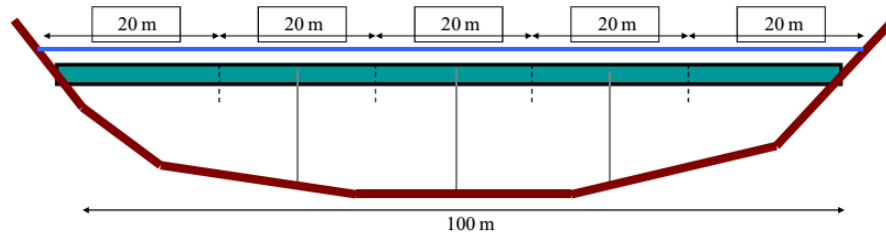


Figure 3.2 Schematic sketch of the SFT prototype ^[12]

The tunnel has a multi-layered cross section that is composed of three different materials. In order to model the “sandwich” style tunnel as a 3D beam, an approach based on equivalence principle of bending stiffness was used by Zhang, Wang, and Hong (2010) to homogenize the three-layered structure. Tunnel’s properties and global equivalent parameters are shown in Table 3.1 and Figure 3.3.

Table 3.1 Equivalent structural parameters of tunnel ^[16]

Structural Parameter	Value	Unit
Density	2018	kg/m ³
Transverse area	5.1	m ²
Area moment of inertia	12.33	m ⁴
Young’s modulus	3.2E+10	N/m ²

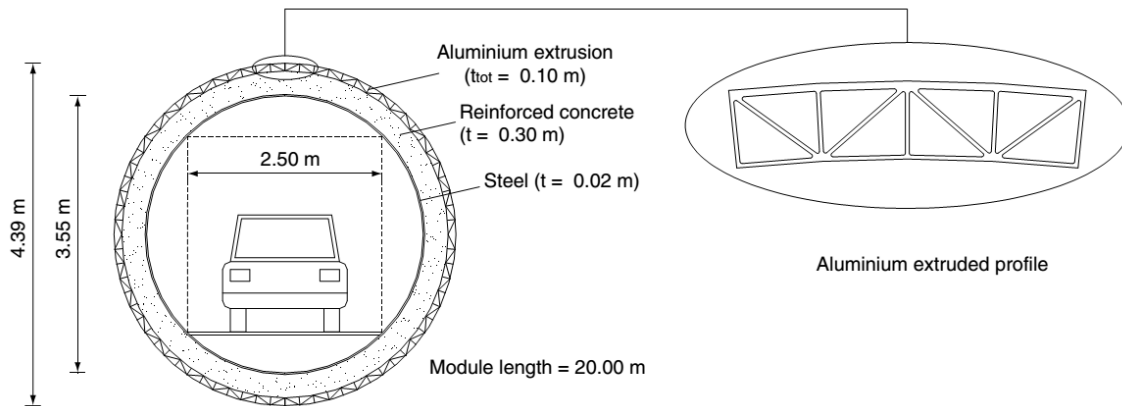


Figure 3.3 The cross section of the SFT prototype [2]

Three cable system configurations are selected for static and dynamic response comparison (See Figure 3.4). From the perspective of safety design requirement, each cable should always be in taut condition to avoid structural failures of other cables. Therefore, it is necessary to determine if slack condition will occur under various environmental loads.

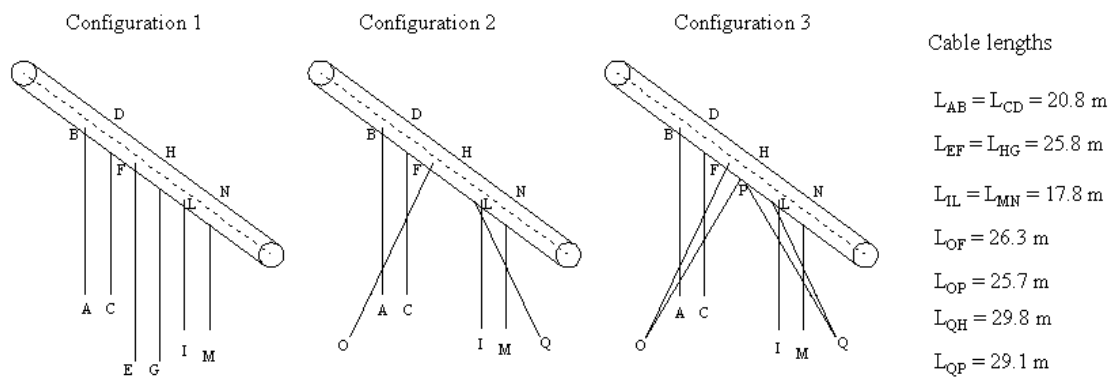


Figure 3.4 Cable configurations for the SFT prototype [12]

Table 3.2 Structural parameters of cable ^[11]

Structural Parameter	Value	Unit
Density	7850	kg/m ³
Transverse area	2.49E-03	m ²
Young's modulus	3.2E+10	N/m ²
Failure load	3140	kN
Design axial load	1045	kN
Inclined angle		
– OF, QL	0.2	rad
– OP, QP	0.4	rad
– Others	0	rad

The structural parameters of cables are shown in Table 3.2. The inclined angle of a cable is defined as the acute angle between the vertical line and the axial direction of the cable. For cables in group 2 of both configuration 2 and configuration 3, they have different lengths and inclined angles, which means cable group 2 is an asymmetric configuration. This asymmetry property results in an unsteady behavior of cable stiffness which will be discussed in Section 3.2.

3.1.2 Fluid properties

The SFT prototype is placed in the water with a submerged depth of 4.2m. The clearance depth is 2m which is defined as the distance between the water surface and the top of the tunnel. The real lake bed profile is uneven as the water depth increases from the two ends of SFT (10m) to the middle of the inlet (30m). However, a constant depth of 30m in the calculation model is utilized to simplify the problem. Other field data of fluid properties are given in Table 3.3.

Table 3.3 Data of fluid environment ^[11]

Fluid Parameter	Value	Unit
Density	1050	kg/m ³
Wave height	1	m
Wave period	2.3	s
Surface current velocity	0.1	m/s
Drag coefficient	1	1
Inertia coefficient	2	1

3.2 Sensitivity Study of Cable Stiffness

To simplify the problem, cables are modeled as equivalent springs to provide restoring forces vertically and horizontally. However, the stiffness of cables is subject to change if the tunnel has significant transverse motion compared to the length of cables. Since the magnitude of tunnel's vertical motion is usually much smaller than its horizontal motion, the following discussion focuses on the behavior of cable stiffness due to tunnel's horizontal motion. Without loss of generality, a single-cable system depicted in Figure 3.5 is used to conduct the sensitivity study.

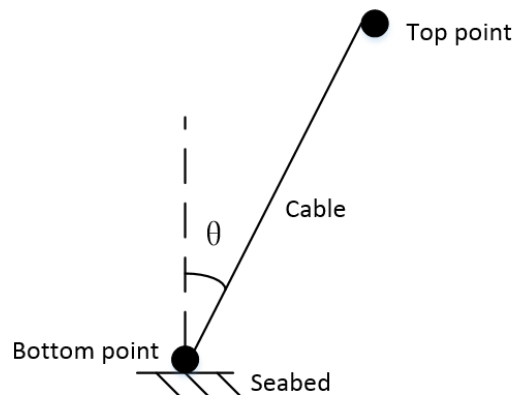


Figure 3.5 Single-cable system for sensitivity study

Table 3.4 Cable Properties

Parameter	Value	Unit
Diameter	60	mm
Length	30	m
Cross-section area	2.49E-03	m ²
Area moment of inertia	6E-07	m ⁴
Young's modulus	1.4E+11	N/m ²
Initial vertical tension component	464.8	kN
Design axial force	1045	kN

Table 3.4 shows the properties of cable in Figure 3.5. The bottom point is anchored to the seabed. The top point is movable horizontally to simulate the tunnel's motion. The initial position of the top point is determined by the static equilibrium position of the tunnel in still water. The inclined angle is set up with different values to analyze its influence on stiffness behavior.

The horizontal and vertical stiffness due to the single-cable system are calculated as follows^[17]:

$$\begin{aligned}
 K_h &= \frac{T \cos^2 \theta}{L} + \frac{EA \sin^2 \theta}{L} \\
 K_v &= \frac{T \sin^2 \theta}{L} + \frac{EA \cos^2 \theta}{L}
 \end{aligned}
 \tag{3.1}$$

where T is the cable axial force, θ is the inclined angle, E is the Young's modulus, A is the cross-section area, L is the length of the cable. Subscripts h and v denote horizontal and vertical component, respectively.

For better comparison, a constant value of the initial vertical tension component is imposed on all the cases in Table 3.5.

Table 3.5 Cases for Sensitivity Study

Case No.	Inclined Angle θ (rad)	θ (deg)
1	0	0
2	0.1	5.7
3	0.2	11.5
4	0.3	17.2

According to Mazzolani et al. (2010), the maximum horizontal motion of the tunnel is always smaller than 0.1m in all three configurations mentioned in Section 3.1.1. Therefore, the range of horizontal displacement for the top point varies from -0.1m to 0.1m. Corresponding variation of horizontal and vertical stiffness are shown in Figure 3.6. (x, y represent tunnel's horizontal displacement and change of stiffness, respectively.)

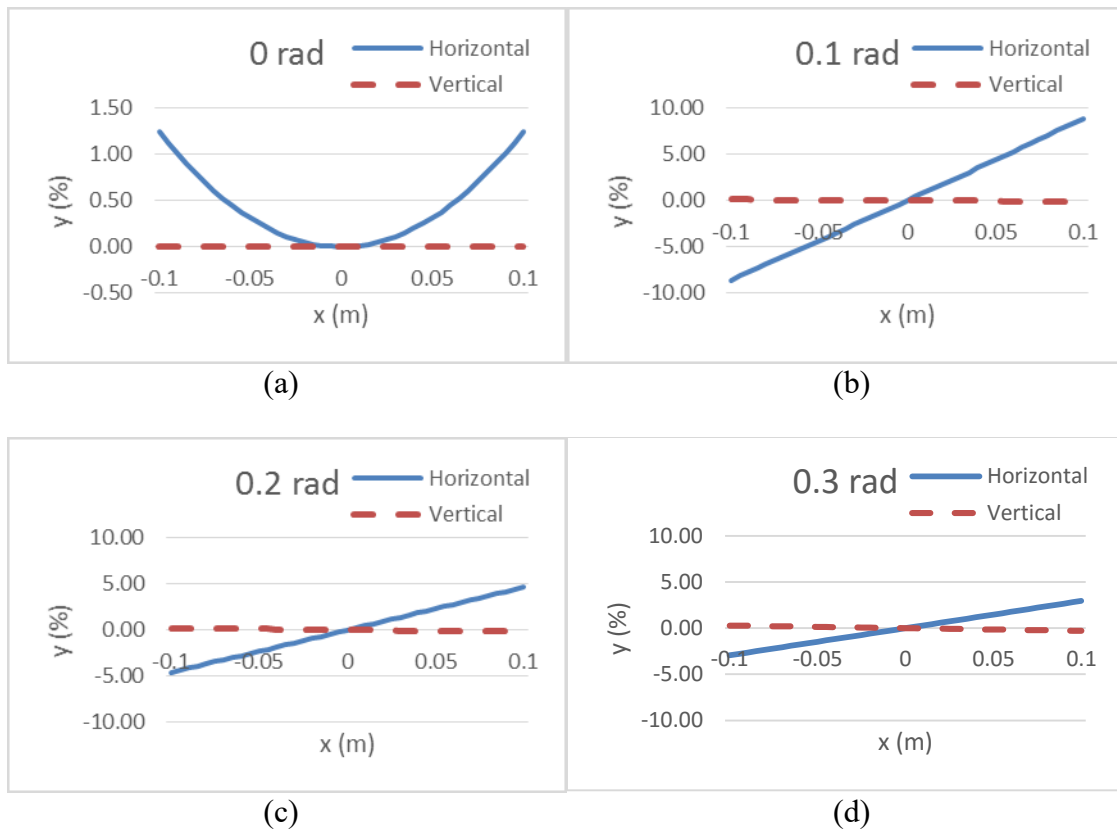


Figure 3.6 Change of horizontal and vertical stiffness due to tunnel's movement

From Figure 3.6, it can be seen that the horizontal stiffness is more sensitive to tunnel's horizontal motion compared with the vertical stiffness. When the cable is initially vertical, its horizontal stiffness follows a parabolic shape due to both positive and negative displacement. However, as the inclined angle increases, the horizontal stiffness tends to behave linearly. For vertical stiffness, it does not change a lot in all cases and the variation is always within $\pm 0.4\%$.

Furthermore, a conclusion can be drawn for cases with symmetric layout of inclined cables. If the tunnel transverse motion is small relative to the length of the cables, the total horizontal stiffness of the cable group can be assumed as a constant due to the aforementioned linear relationship. For symmetric system with vertical cables, the horizontal stiffness shows parabolic behavior with its smallest value when the horizontal displacement is zero. For system with asymmetric cable setup, the horizontal stiffness can either be linear or nonlinear, which depends on the configuration of each cable and the amplitude of tunnel motion.

3.3 Numerical Implementation

For each cable system configuration, a three-dimensional finite element model of the SFT prototype in Qiandao Lake is constructed in Matlab. Also, a corresponding structural model is built in ABAQUS for comparison with Matlab. Unlike the full finite element model approach in ABAQUS, cables are transformed into equivalent springs in the Matlab implementation for each iteration of calculation. This strategy is employed to accelerate the solving process and is extremely convenient when it comes to parametric

study of cable system configurations. A schematic sketch of the SFT prototype with configuration 3 is shown in Figure 3.7.

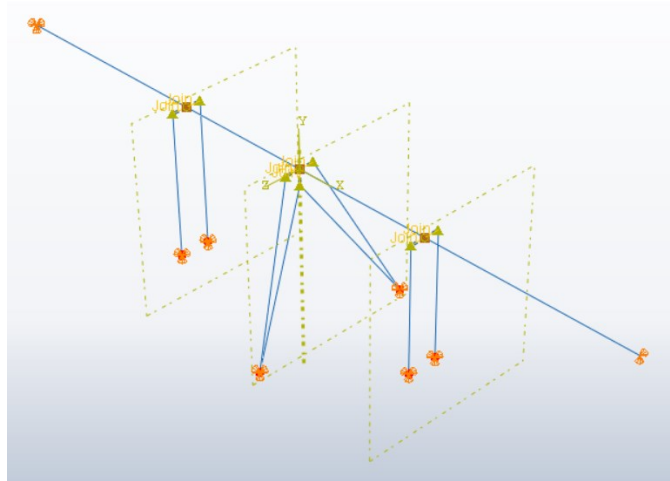


Figure 3.7 Sketch of SFT (Config. 3) in ABAQUS

In ABAQUS, the two ends of the tunnel have different boundary conditions. The upper left end is modeled as a hinge with free rotation while the lower right end has an additional degree of freedom in the axial direction of the tunnel. For cables, all the bottom anchored points and top points are also modeled as hinges. Joint connectors are created to ensure all top cable points are following the corresponding sectional displacements of the tunnel. The tunnel is meshed with 3-node quadratic beam elements and each cable is modeled as a 2-node linear truss element.

In Matlab, the tunnel is discretized into 2-node linear beam elements. With convergence tests conducted, the element size is set to be 1m and hence the total number of beam elements is 100. Each configuration has three cable groups. A cable group can be

represented by a pair of horizontal and vertical springs. Within each iteration of calculation, the spring stiffness is updated and added to the SFT stiffness matrix. The finite element model in Matlab is schematically depicted in Figure 3.8.

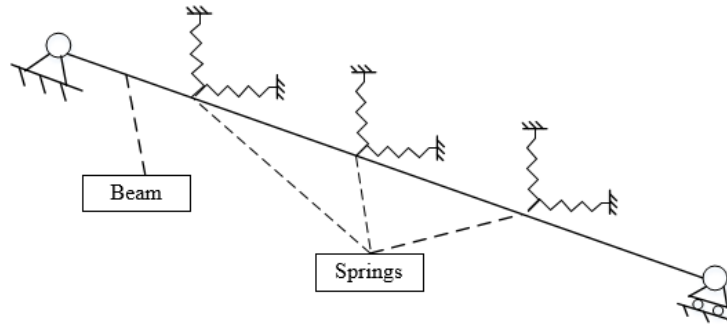


Figure 3.8 Sketch of SFT model in Matlab

The methodology formulated in Section 2 is to be implemented in Matlab using the flow chart presented in Figure 3.10.

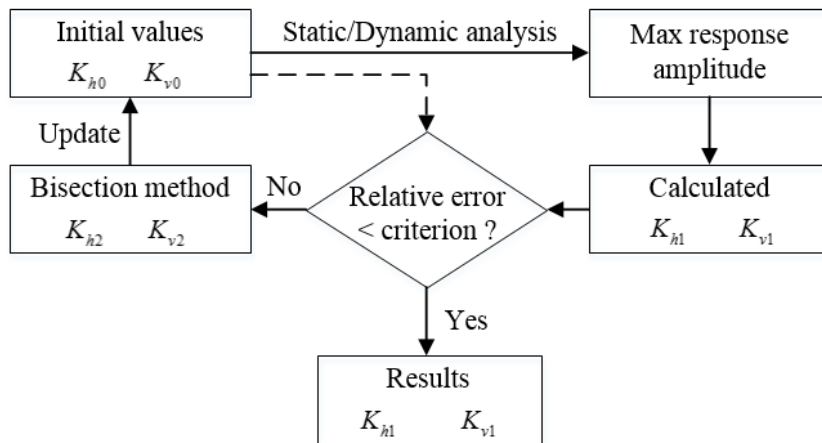


Figure 3.9 Flow chart of stiffness convergence with bisection method

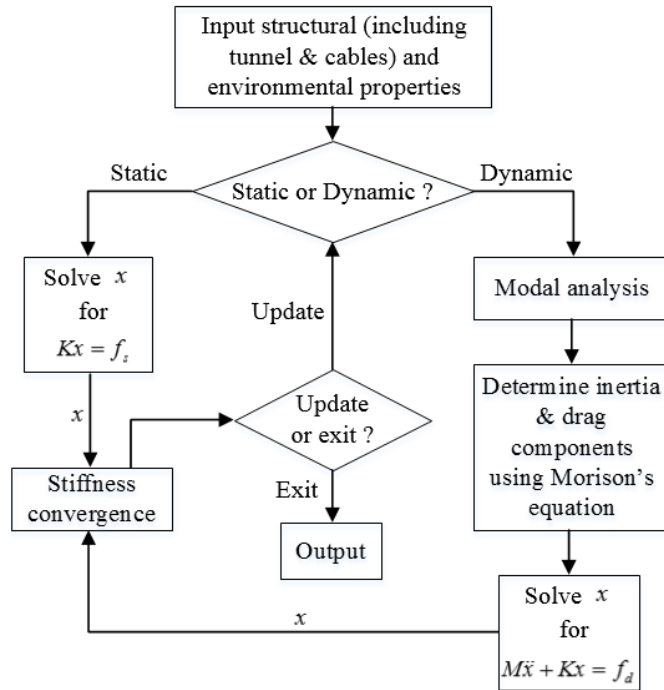


Figure 3.10 Flow chart of numerical analysis in Matlab

For both static and dynamic calculations, a bisection method is introduced to repeatedly capture the variation of cable stiffness and to obtain an approximate solution. This method starts from the initial condition of SFT under still water. Each cable group has a set of equivalent initial horizontal and vertical stiffness denoted as K_{h0} and K_{v0} , respectively. These stiffness are used to determine the response of SFT under environmental loads. Once the response amplitude is known, the corresponding horizontal and vertical stiffness of each cable group, denoted K_{h1} and K_{v1} , are calculated and compared to K_{h0} and K_{v0} . If the difference does not satisfy the specified convergence criterion, K_{h2} and K_{v2} will be determined based on the mean position of the previous two

results, and will replace K_{h0} and K_{v0} as the new initial values for the next iteration. Loops of calculation are executed until the relative error is sufficiently small. See Figure 3.9 for stiffness convergence and Figure 3.10 for Matlab implementation.

3.4 Program Validation

Both static and dynamic analyses of the SFT prototype are conducted in the Matlab program and the results are compared with full FEM in ABAQUS and publications from SIJLAB^[12]. Three cable system configurations (refer to Figure 3.4) are also compared in terms of maximum structural response. Finally, maximum cable axial forces are determined to assess the performance of cable system.

3.4.1 Static calculation

For static cases, drag and inertia components due to both current and waves are evaluated as “static” values. The resultant horizontal and vertical hydrodynamic forces are 4.875 kN/m and 4.860 kN/m, respectively. Besides, buoyancy and gravitational loads are also added to the vertical component. The sketch of forces acting on the SFT with configuration 3 is shown in Figure 3.11.

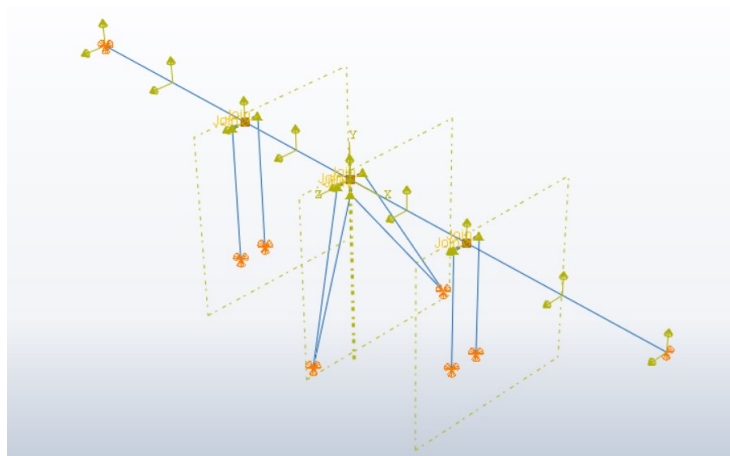


Figure 3.11 Illustration of static force on SFT

Static calculations are conducted in Matlab and ABAQUS, respectively. Figure 3.12 to Figure 3.14 show the numerical results for three different cable configurations. For each configuration, figure (a) shows the static horizontal response; figure (b) shows the static vertical response; figure (c) shows the static total response. Refer to Figure 3.4 for structural parameters of three cable system configurations.

For configuration 1:

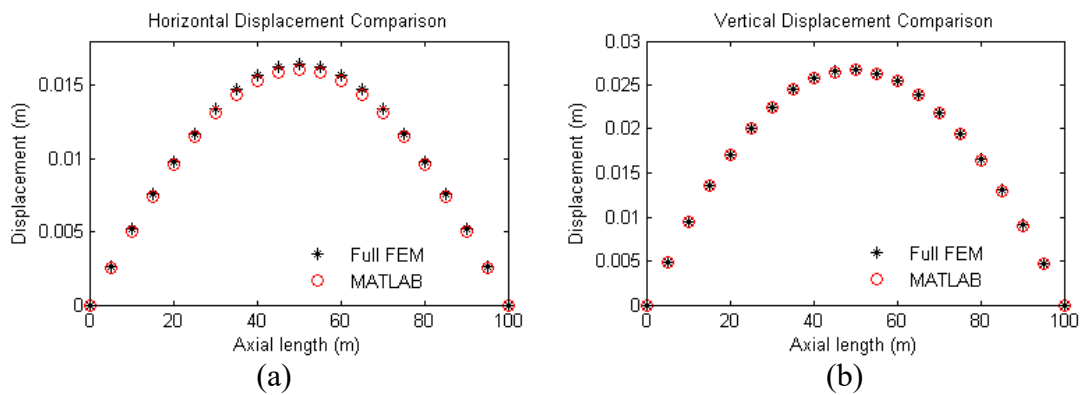
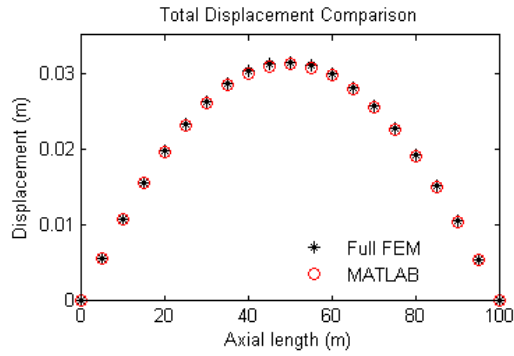


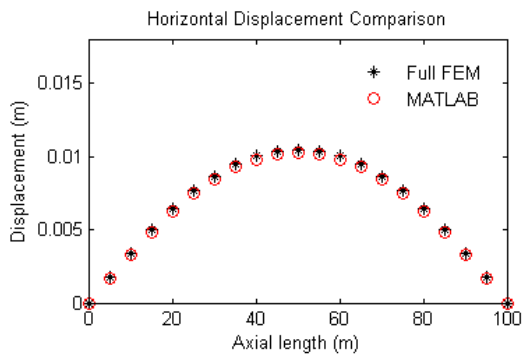
Figure 3.12 Static results of configuration 1



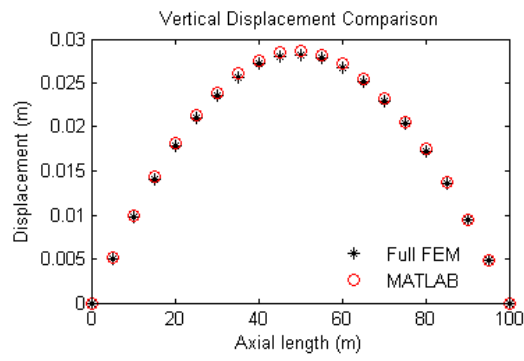
(c)

Figure 3.12 (Continued)

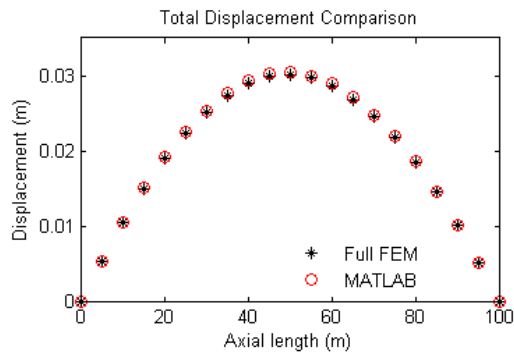
For configuration 2:



(a)



(b)



(c)

Figure 3.13 Static results of configuration 2

For configuration 3:

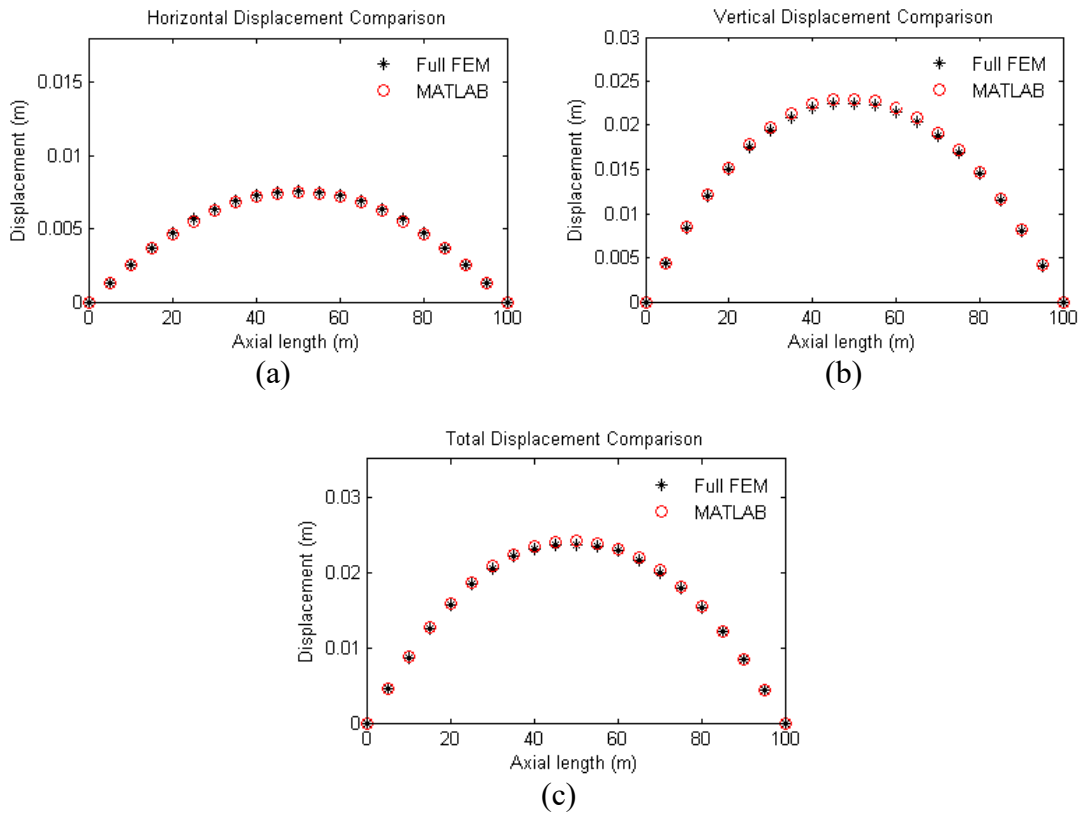


Figure 3.14 Static results of configuration 3

In Table 3.6, “V” denotes vertical, “H” denotes horizontal, and “Mag.” denotes total magnitude. Results of displacements under static loads from the Matlab program show pretty good agreement with those obtained by full FEM in ABAQUS. Although little discrepancy is observed between the Matlab program and the SIJLAB research group, this error is expected and acceptable because a simplified model was used in the former approach. In addition, selections of different types of beam elements and meshing density can also contribute to the variation in the results.

Table 3.6 Summary of maximum displacement (m) comparison

(a) Full FEM in ABAQUS								
Configuration 1			Configuration 2			Configuration 3		
V	H	Mag.	V	H	Mag.	V	H	Mag.
0.027	0.016	0.031	0.028	0.010	0.030	0.022	0.008	0.024

(b) Matlab Program								
Configuration 1			Configuration 2			Configuration 3		
V	H	Mag.	V	H	Mag.	V	H	Mag.
0.027	0.016	0.031	0.029	0.010	0.030	0.023	0.007	0.024

(c) SIJLAB Research Group								
Configuration 1			Configuration 2			Configuration 3		
V	H	Mag.	V	H	Mag.	V	H	Mag.
0.027	0.018	0.033	0.030	0.012	0.032	0.025	0.008	0.026

3.4.2 Dynamic calculation

Environmental conditions specified in Section 3.1.2 are imposed on the SFT prototype. Airy wave theory is used to evaluate horizontal and vertical fluid velocities and accelerations. The drag term and added mass are derived from Morison's equation for each sectional element. The dynamic response is solved in frequency domain. The total response is assumed to be the sum of the static response and the dynamic response. From Figure 3.15 to Figure 3.17, results of the dynamic response of tunnel are shown in which monochromatic waves are generated and they are traveling perpendicular to the tunnel axial direction. As the same practice in static calculation, three cable system configurations are calculated and compared with each other to better evaluate its position keeping performance.

For configuration 1:

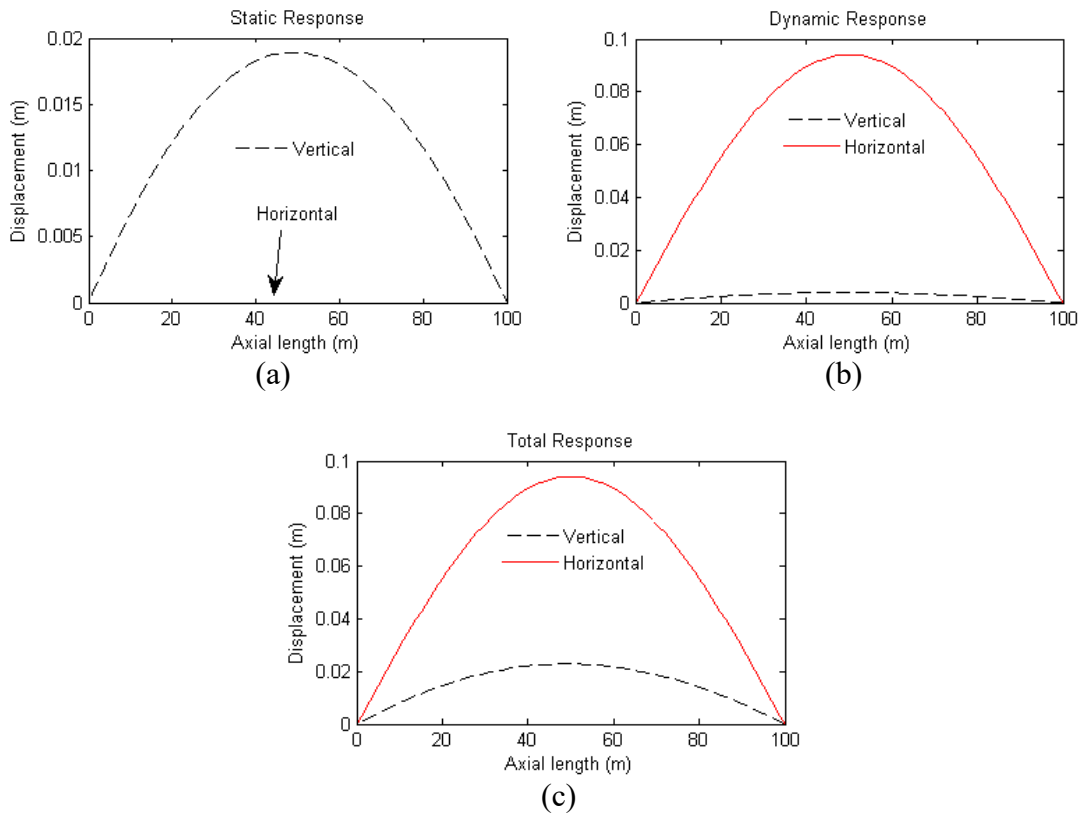


Figure 3.15 Dynamic results of configuration 1

For configuration 2:

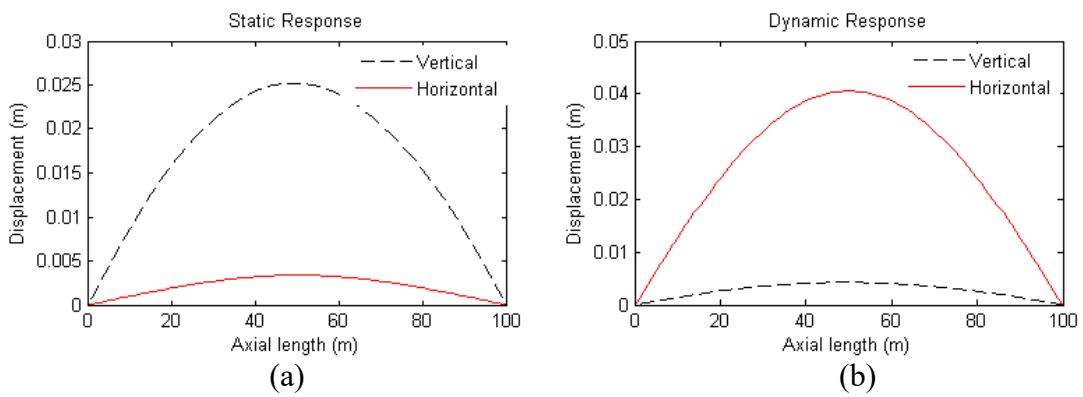


Figure 3.16 Dynamic results of configuration 2

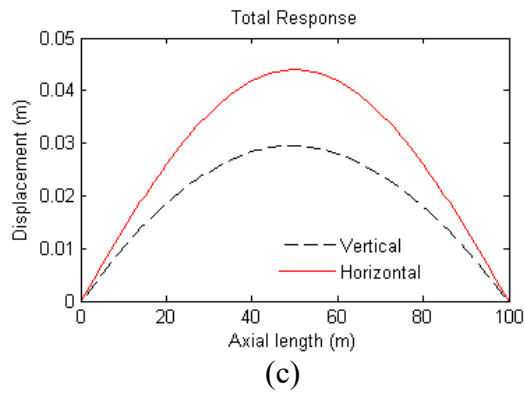


Figure 3.16 (Continued)

For configuration 3:

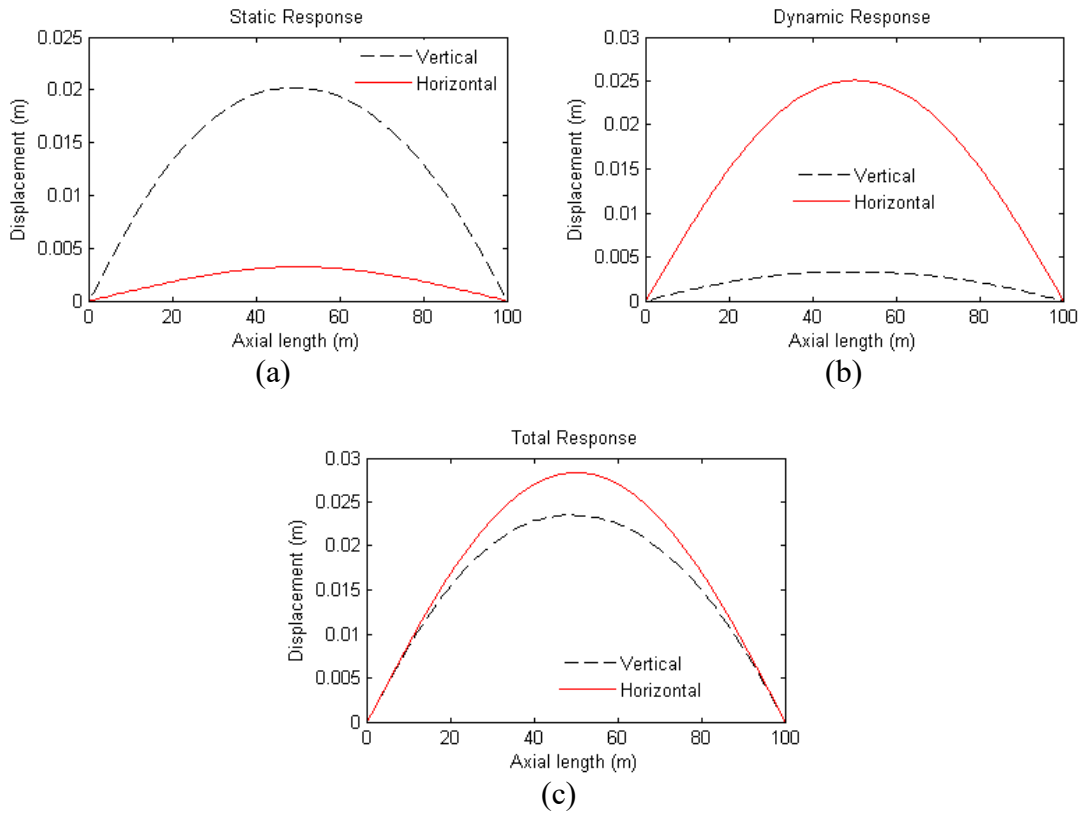


Figure 3.17 Dynamic results of configuration 3

Table 3.7 Summary of response magnitude comparison

	Displacement (m)	Matlab program	SIJLAB
Configuraion 1	Horizontal	0.094	0.092
	Vertical	0.023	0.019
	Total	0.097	0.094
Configuraion 2	Horizontal	0.044	0.040
	Vertical	0.029	0.029
	Total	0.053	0.049
Configuraion 3	Horizontal	0.028	0.025
	Vertical	0.023	0.022
	Total	0.037	0.034

Results predicted by the Matlab program again give good agreement with the values by SIJLAB (See Table 3.7), although the former ones are either equal to or slightly larger than the latter ones. This difference is small compared with the magnitude itself. Several modeling issues could lead to this discrepancy. One is the stiffness convergence algorithm as shown in Figure 3.9. While it gives very accurate results for static calculations, it could possibly neglect some non-linearities that might increase the equivalent stiffness due to cable system. Another aspect is the assumption of the total response. In the Matlab program, the static response and the dynamic response are added together linearly to get the total response. This neglects the coupling effect between the static and dynamic calculation in terms of cable stiffness.

The SFT model with configuration 3 has the smallest horizontal and vertical response amplitude while the model with configuration 1 has the largest. This reduction in response is achieved by adding two more cables to cable group 2 and making the cables inclined appropriately. Inclined cables are more effective in increasing the horizontal

stiffness of SFT. For example, the equivalent horizontal stiffness for cable group 2 in configuration 1 is $2.94E+04$ N/m while that in configuration 3 is $9.66E+06$ N/m.

From Table 3.6 and Table 3.7, it can also be observed that the response amplitudes are much larger in dynamic calculations than in static calculations. The reason lies in the fact that the structural acceleration was not taken into account in static cases. Since the added mass coefficient is 1, the fluid forces generated by the tunnel's motion can increase the total force significantly when the relative acceleration is larger than the amplitude of the fluid acceleration itself. Therefore, it is undoubtedly necessary to conduct dynamic analyses of SFTs as oppose to static calculations because static predictions would generally underestimate the forces and hence displacements.

4. APPLICATION

4.1 Project Description

Over the past 20 years, the society of SFT research in Hokkaido has carried out a variety of feasibility studies of various SFT projects in Japan from numerical simulations to experiments. These proposed applications cover a wide range of design purposes, crossing distances, and water depths. See Table 4.1.

Table 4.1 Major feasibility studies done by the society of SFT research in Hokkaido ^[3]

Name	Location	Purpose	Length (m)	Max. Water Depth (m)
Funka Bay Crossing	Bay threshold	Motor vehicle Railroad	30,000	120
Toya Lake Crossing	Lake crossing	Pedestrian Mono-rail	3,000	100
Rishiri Rebun Crossing	Strait Crossing	Lifeline Transportation	22,000	200
Ishikariwan Shinko In-port Crossing	In-port Crossing	Motor vehicle	972	15
Daikokujima Crossing	In-port Crossing	Pedestrian	120	10
Soya Strait Crossing	Strait Crossing	Motor vehicle Railroad	43,000	180
Otaru In-port Crossing	In-port Crossing	Pedestrian	300	10

The Otaru In-port Crossing project is specifically selected as the application of the methodology developed in Chapter 2 for two reasons. First, it is a pedestrian-aimed SFT with a crossing distance of 300m, which is longer than the SFT prototype in Qiandao Lake. The characteristic of slenderness is more dominant in this case with larger aspect ratio. Second, it is located in a relatively shallow water region with maximum water depth of

10m. The horizontal motion of the SFT is more vulnerable to surface waves due to the elliptical water particle trajectories throughout the water column. Conversely the water depth of the Qiandao Lake is 30m. In this case surface waves have less influence if the SFT is submerged deep enough in the water.



Figure 4.1 Location of Otaru In-port Crossing SFT

4.2 Wave Conditions

According to the wave statistics provided by Windfinder^[18], the typical wave height and wave length in service condition are 0.9m and 22m, respectively. Because the axial direction of the SFT is approximately parallel to the shoreline (See Figure 4.1), it is assumed that waves are travelling perpendicular to the longitudinal direction of the tunnel.

4.3 Structural Model

Structural dimensions and properties of this pedestrian-aimed SFT in Otaru are designed based on the previous study of the SFT prototype in Qiandao Lake. Detailed parameters are shown in Figure 4.2.

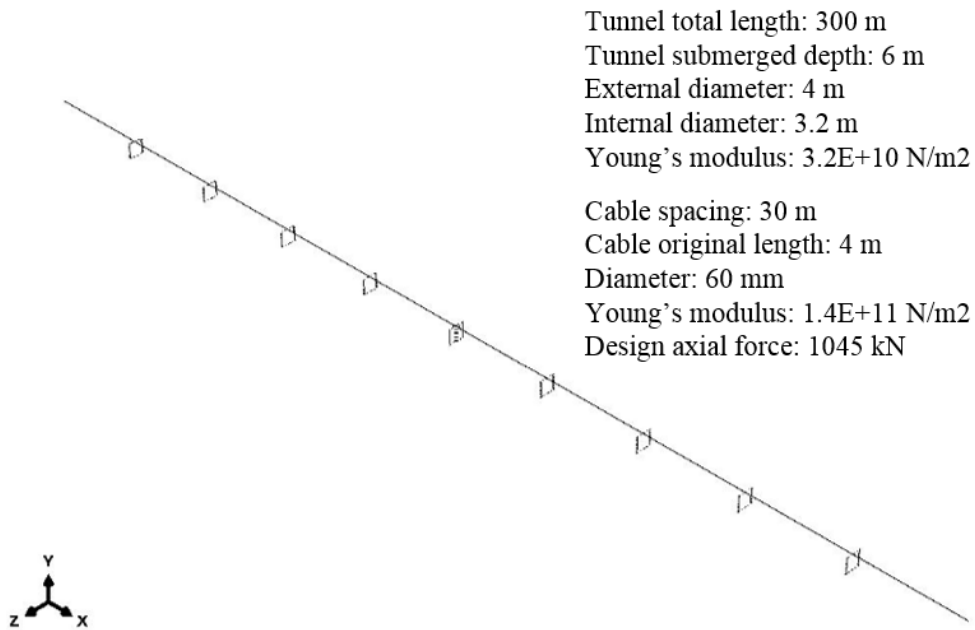


Figure 4.2 Structural parameters of SFT in Otaru

The proposed SFT has 9 cable groups distributed evenly along the tunnel. Each cable group has two vertical cables with unstretched length of 4m. The material and cross-section properties of these cables remain the same as mentioned in Table 3.2. Tunnel's cross section is still a "sandwich" type multi-layered structure and its equivalent parameters are calculated based on the equivalent principle of bending stiffness mentioned in Section 3.1.1. See Table 4.2.

Table 4.2 Equivalent structural parameters of SFT in Otaru

Structural Parameter	Value	Unit
Density (with live loads)	2200	kg/m ³
Transverse area	4.5	m ²
Area moment of inertia	7.42	m ⁴
Young's modulus	3.2E+10	N/m ²

The tunnel is discretized into 2-node linear beam elements. The element size is set to 3m after convergence tests. All cables are modeled as springs with initial stiffness values obtained from results in still water. One end of the tunnel is a hinge connection and the other end has an axial relaxation device.

4.4 Dynamic Response under Monochromatic Waves

The three-dimensional finite element model of the SFT and the monochromatic waves specified in Section 4.2 are simulated in the Matlab program. The results of static, dynamic, and total response are shown in Figure 4.3.

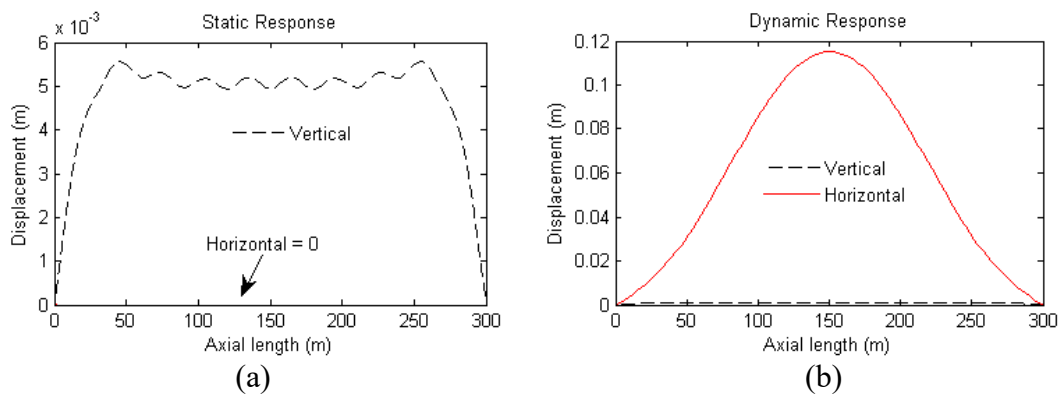


Figure 4.3 Dynamic results of proposed SFT in Otaru

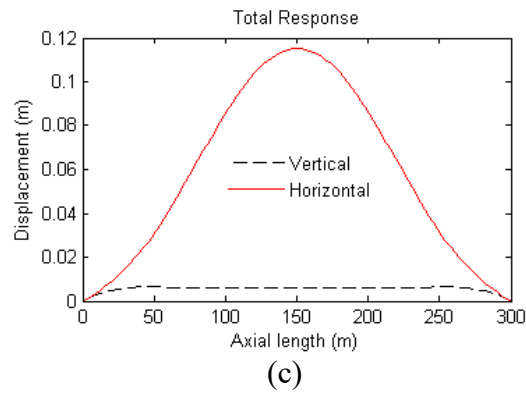


Figure 4.3 (Continued)

The total horizontal response is much larger than the total vertical response. The amplitude of the vertical response is only 5.7% of the horizontal response. The vertical response is restrained to a small value (0.007m) by the presence of cables distributed along the tunnel. From Section 3.2, it is observed that a vertical cable provides less horizontal stiffness to the tunnel than an inclined cable. This is generally true if the horizontal motion of the SFT is negligible compared to the length of the cable. In the case of Otaru SFT, the length of cables is restricted by the 10m water depth. The effects of short inclined cables on the SFT behavior is of great interest and will be investigated in Section 4.5.

Since the dynamic response is calculated based upon the contributions from selected modes, it is important to determine whether enough mode components have been selected to well represent the SFT behavior. As stated in Equation (2.10) in Section 2.3, \bar{p}^e is a vector whose magnitude reflects the contribution from each mode. With that determined from previous calculation, the percentage that each mode accounts for in the total horizontal response can be shown in Figure 4.4.

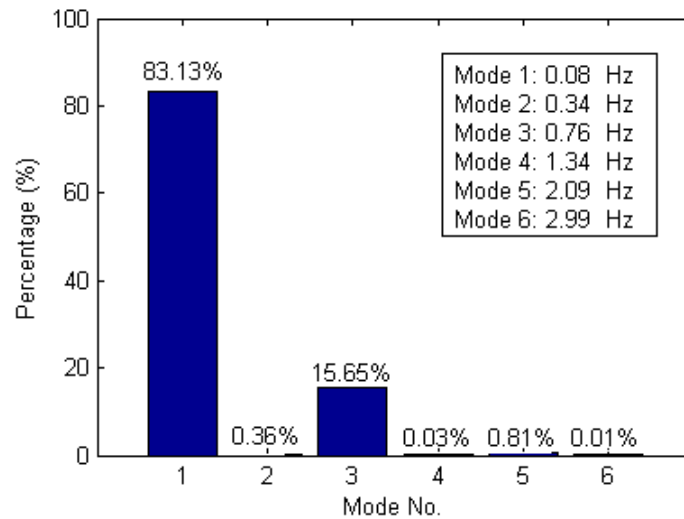


Figure 4.4 Mode percentage in horizontal response

The wave frequency corresponding to the 22m wave length is 0.27 Hz, which lies between the first two natural frequencies of the SFT. The first and third natural modes together account for over 98.7% while the second natural mode only contributes 0.36%. For odd number modes, the mid-span of the SFT has the largest amplitude, which is indicated in previous calculations. However, for even number modes, the mid-span is a node with zero amplitude. This discrepancy gives rise to the large contributions from odd number modes and small contributions from even number modes.

With maximum horizontal and vertical displacement determined, the maximum axial forces of mooring cables can also be evaluated. The failure load for each cable is 3140 kN. With a safety factor of 3, the corresponding design value is 1045 kN. This design value will be indicated as a horizontal red dash line in the following figures of cable tension variation.

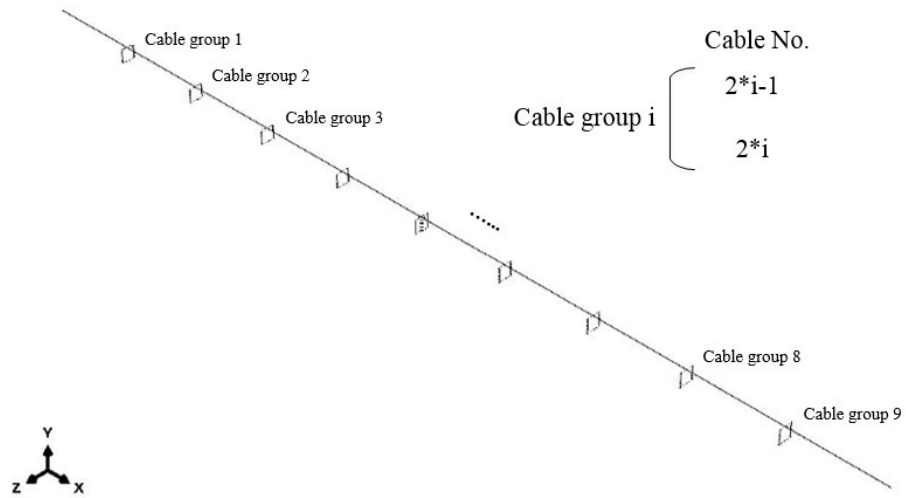


Figure 4.5 Cable group and cable number assignments

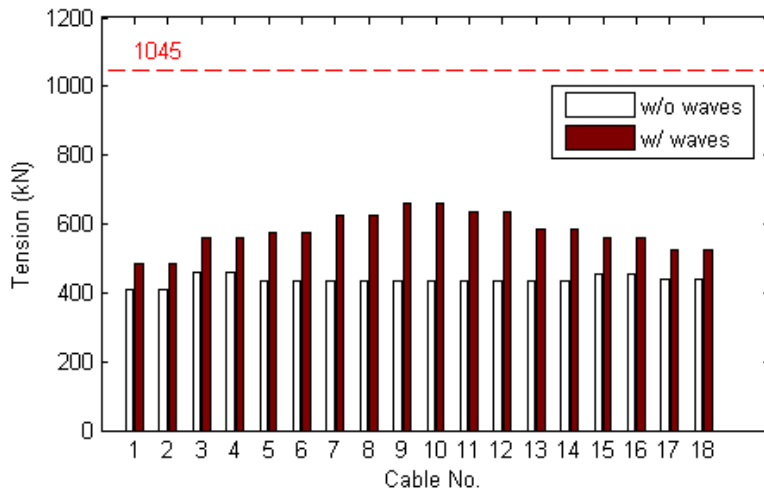


Figure 4.6 Variation of cable tension

Figure 4.5 shows the cable and cable group numbering for the Otaru SFT. In Figure 4.6, the white bars indicate the cable tension in still water and the solid bars represent the maximum cable tension under surface waves. Attention should be given to cables

distributed around the mid-span of SFT. These cables have the largest displacement and therefore, variation compared with those near the two ends. The maximum tension occurring at Cable No.9 and No.10 is about 62% of the design value (1045 kN), which is high as the cables might have larger tension variation as the SFT undergoes more severe environmental conditions. More cables and better configuration scheme are needed to enhance the structural integrity of the SFT.

4.5 Parametric Study

This section investigates the effects of two fundamental parameters on the dynamic response of Otaru SFT in wave fields. First, the cables located at the mid-span of the tunnel are inclined to different angles. All the other cables remain the same configuration as in Figure 4.5. Second, the SFT is set up with different submerged depths. The length of cables is adjusted according to the submerged depth so that all cables are vertically configured.

The structural model described in Section 4.3 serves as the base model of the parametric study. Details of other models with different setup are shown in Table 4.3.

Table 4.3 Cases for parametric study

Case No.	Description
0	Base model; mid-span cables are vertical; tunnel submerged depth = 6 m
1	Mid-span cables are inclined with angle of 0.1 rad
2	Mid-span cables are inclined with angle of 0.2 rad
3	Tunnel submerged depth = 4 m
4	Tunnel submerged depth = 5 m
5	Tunnel submerged depth = 7 m

All cases are simulated in the Matlab program with the same surface wave condition given in Section 4.2. The horizontal response and cable tension variation are compared and shown as follows.

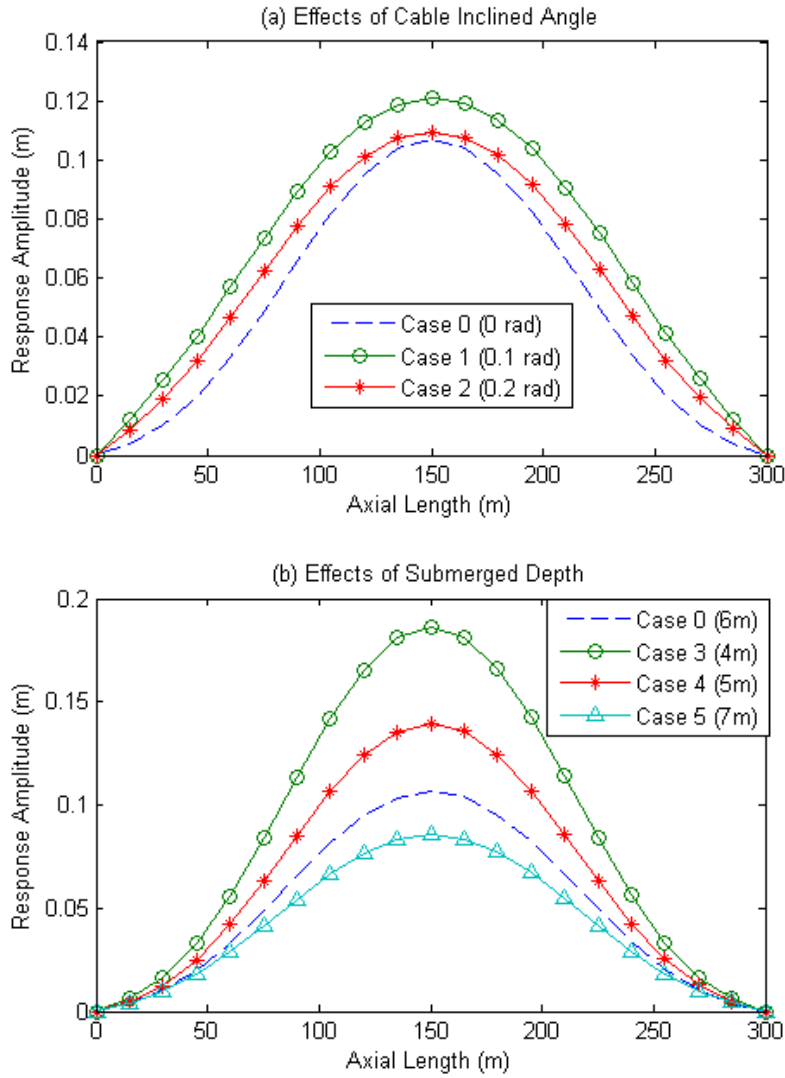


Figure 4.7 Comparison of horizontal response

It is observed in Table 3.7 that inclined cables can provide larger horizontal stiffness to SFTs compared to vertical cables. However, in Figure 4.7 (a), for inclined angle configuration, the horizontal response amplitude along the tunnel is larger than base case. The underlying reason is the presence of slack cables, which is illustrated in Figure 4.8.

From Figure 4.7 (b), it is obvious that the influence of the submerged depth on the horizontal response of SFT is significant. There are two main reasons. First, as the SFT gets closer to the water surface, the larger the hydrodynamic forces become. Second, provided the tension of each cable remains the same, the longer the vertical cable, the lesser horizontal stiffness it can offer according to Equation (3.1).

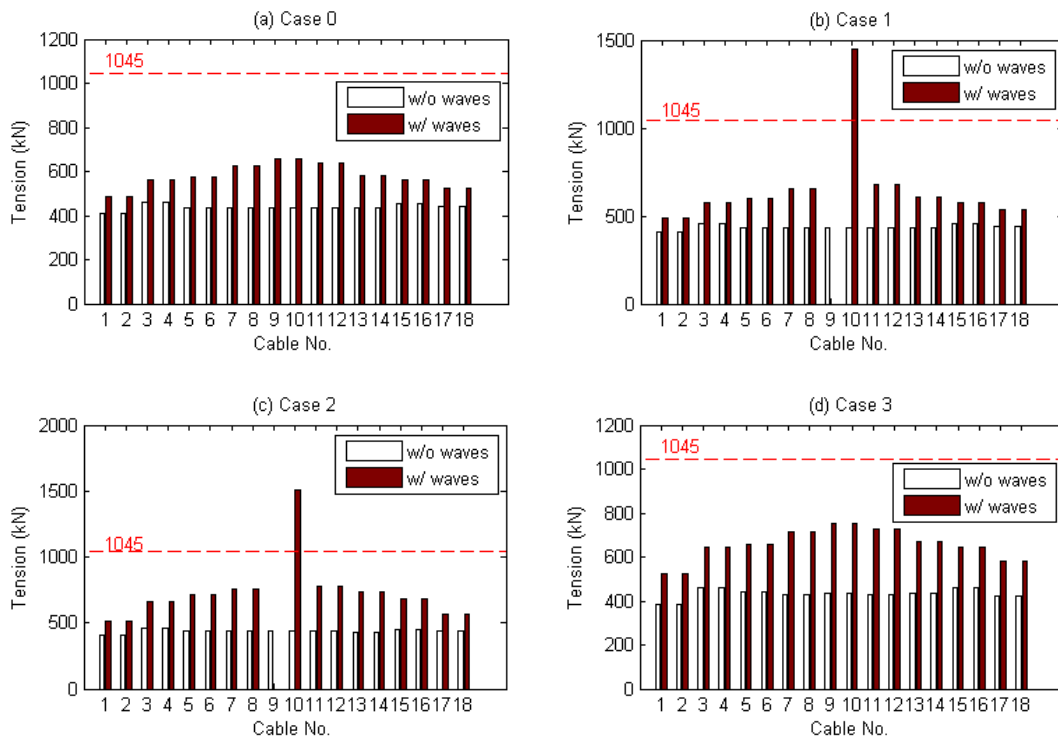


Figure 4.8 Comparison of cable tension variations

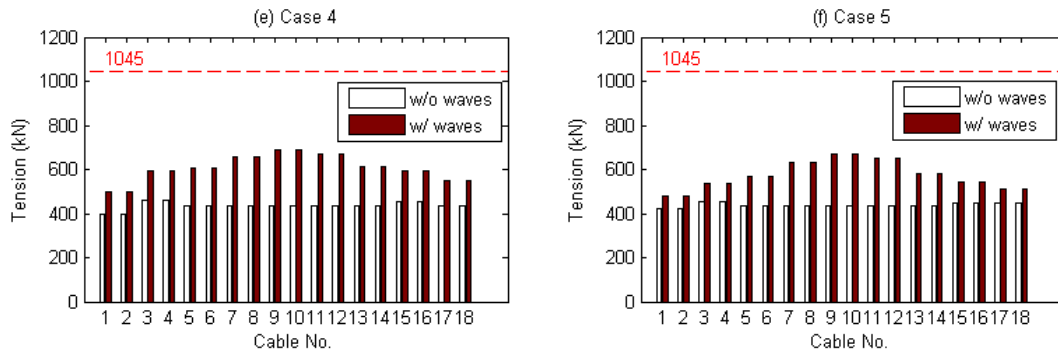


Figure 4.8 (Continued)

In both Case 1 and Case 2, the tension of the cable located at the mid-span exceeds the design value (1045kN) due to the presence of a slack cable in the same group. The cable with the zero tension can be regarded as the slack cable. Since the slack cable cannot contribute to the horizontal stability of the SFT, the adjacent cable has to bear much larger tension to stabilize the SFT motion. The occurrence of slack conditions should be avoided to prevent failure of cables. Slack cables are more likely to happen in cases where short inclined cables are used in shallow water regions, especially when the SFT motion is no longer much smaller than the length of cables.

The results from Case 3 to Case 5 are expected from previous analysis. Case 3 has the largest response amplitude and cable tension variation as it is undergoing the largest hydrodynamic forces. Case 5, on the other hand, has the smallest values as it has the largest submerged depth.

5. SUMMARY

Although the evaluations of wave forces on submerged floating tunnels (SFTs) have been studied for many years, a computationally efficient and robust solving technique is still needed for initial investigation of anchoring system performance and structural parametric study. With this aim, a frequency-domain approach utilizing both the Morison's equation and mode decomposition was proposed in this research investigation. The main objective of this research study was to formulate the procedure of building hydroelastic model of SFTs and to validate the proposed methodology.

In order to analyze the hydrodynamic behavior of the SFT prototype under monochromatic surface waves in Qiandao Lake, a three-dimensional finite element hydroelastic model was first constructed. In this model, linear beam elements were adopted to mimic the slender behavior of the tunnel. The anchoring system was represented by horizontal and vertical springs with equivalent stiffness. A sensitivity study of cable stiffness was performed to better understand the influence of tunnel's motion. Results showed horizontal stiffness was more sensitive and its value was also affected by the cable's inclined angle. As part of the numerical program, a bisection method was introduced to guarantee and accelerate the convergence of stiffness calculations. Both static and dynamic predictions by the proposed methodology showed good agreement with results from SIJLAB in terms of horizontal and vertical response amplitude.

The methodology developed in this study was further applied to investigate the structural response of the Otaru In-port crossing SFT. In this design, all of the anchoring

lines were vertical and evenly distributed along the length of the 300m long tunnel. The total response of the tunnel under service wave conditions provided by Windfinder was obtained by summing the static and dynamic response contributions. For the safety requirement, the maximum axial force for each anchoring line was calculated with respect to the total response amplitude. Contributions of different modal components to the total response were also determined in order to check whether adequate mode shapes had been selected. Parametric studies based on this generic model were conducted in terms of cable inclined angle and tunnel submerged depth. As the tunnel gets closer to the water surface, the SFT undergoes increasing hydrodynamic forces as expected. Results also suggest in shallow water areas where cable length is confined to a small value, inclined cable configurations should be used with caution as slack conditions might happen which leads to high tension and failure to adjacent anchoring lines.

In summary, the proposed hydroelastic model and methodology can well predict the dynamic response of SFTs under monochromatic waves. It provides a fast and accurate approach to analyze the hydroelasticity of SFTs from the perspective of modal analysis. As a computationally efficient procedure, it possesses great advantages in terms of global anchoring system selection and structural parametric study. As part of the future work, this methodology will be extended to irregular waves by using linear system approach. Spectral analysis can then be implemented to evaluate the dynamic response of SFTs in frequency domain. In addition, the effects of current and structural radiation should be taken into account for better predictions of structural response in various environmental conditions.

REFERENCES

- [1] B. Jakobsen, “Design of the Submerged Floating Tunnel operating under various conditions,” *Procedia Eng.*, vol. 4, no. 1877, pp. 71–79, Jan. 2010.
- [2] F. M. Mazzolani, R. Landolfo, B. Faggiano, M. Esposto, F. Perotti, and G. Barbella, “Structural Analyses of the Submerged Floating Tunnel Prototype in Qiandao Lake (PR of China),” *Adv. Struct. Eng.*, vol. 11, no. 4, pp. 439–454, Aug. 2008.
- [3] S. Kanie, “Feasibility studies on various SFT in Japan and their technological evaluation,” *Procedia Eng.*, vol. 4, pp. 13–20, 2010.
- [4] Y. Wu, “Hydroelasticity of floating bodies.” University of Brunel, London, UK, 1984.
- [5] W. G. Price and Y. Wu, “Hydroelasticity Of Marine Structures,” Cambridge University Press, Cambridge, UK, 1986.
- [6] R. E. D. Bishop, W. G. Price, and Y. Wu, “A General Linear Hydroelasticity Theory of Floating Structures Moving in a Seaway,” *Philos. Trans. R. Soc. A Math. Phys. Eng. Sci.*, vol. 316, no. 1538, pp. 375–426, Apr. 1986.
- [7] J. N. Newman, “Wave effects on deformable bodies,” *Appl. Ocean Res.*, vol. 16, no. 1, pp. 47–59, Jan. 1994.
- [8] F. Ge, W. Lu, X. Wu, and Y. Hong, “Fluid-structure interaction of submerged floating tunnel in wave field,” *Procedia Eng.*, vol. 4, pp. 263–271, Jan. 2010.
- [9] I. Y. Paik, C. K. Oh, J. S. Kwon, and S. P. Chang, “Analysis of wave force induced dynamic response of submerged floating tunnel,” *KSCE J. Civ. Eng.*, vol. 8, no. 5, pp. 543–550, Sep. 2004.
- [10] F. Brancaloni and A. Castellani, “The response of submerged tunnels to their environment,” vol. 11, pp. 47–56, 1989.
- [11] X. Long, F. Ge, L. Wang, and Y. Hong, “Effects of fundamental structure parameters on dynamic responses of submerged floating tunnel under hydrodynamic loads,” *Acta Mech. Sin.*, vol. 25, no. 3, pp. 335–344, Feb. 2009.
- [12] F. M. Mazzolani, B. Faggiano, and G. Martire, “Design aspects of the AB prototype in the Qiandao Lake,” *Procedia Eng.*, vol. 4, pp. 21–33, 2010.

- [13] H. Kunisu, "Evaluation of wave force acting on Submerged Floating Tunnels," *Procedia Eng.*, vol. 4, pp. 99–105, Jan. 2010.
- [14] Abaqus 6.14 Documentation. <http://server-afb147.ethz.ch:2080/v6.14/index.html>. Accessed March 3, 2015.
- [15] J. R. Morison, J. W. Johnson, and S. a. Schaaf, "The Force Exerted by Surface Waves on Piles," *J. Pet. Technol.*, vol. 2, no. 5, pp. 149–154, 1950.
- [16] S. Zhang, L. Wang, and Y. Hong, "Structural analysis and safety assessment of submerged floating tunnel prototype in Qiandao Lake (China)," *Procedia Eng.*, vol. 4, pp. 179–187, Jan. 2010.
- [17] S. Remseth, B. J. Leira, K. M. Okstad, and K. M. Mathisen, "Dynamic response and fluid / structure interaction of submerged floating tunnels," vol. 72, 1999.
- [18] Wind, waves & weather forecast Otaru - Windfinder. <http://www.windfinder.com/forecast/otaru>. Accessed April 4, 2015.